AIP | Applied Physics Letters

# High temperature, single mode, long infrared (=17.8m) InAs-based quantum cascade lasers

D. Chastanet, A. Bousseksou, G. Lollia, M. Bahriz, F. H. Julien, A. N. Baranov, R. Teissier, and R. Colombelli

Citation: Applied Physics Letters **105**, 111118 (2014); doi: 10.1063/1.4895763
View online: http://dx.doi.org/10.1063/1.4895763
View Table of Contents: http://scitation.aip.org/content/aip/journal/apl/105/11?ver=pdfcov
Published by the AIP Publishing

**Articles you may be interested in**

Long-infrared InAs-based quantum cascade lasers operating at 291K (=19m) with metal-metal resonators
Appl. Phys. Lett. **104**, 021106 (2014); 10.1063/1.4861465

Surface emitting quantum cascade lasers operating in continuous-wave mode above 70°C at 4.6m
Appl. Phys. Lett. **103**, 041121 (2013); 10.1063/1.4816722

Distributed feedback quantum cascade lasers at 13.8 m on indium phosphide
Appl. Phys. Lett. **98**, 211118 (2011); 10.1063/1.3593499

Room-temperature, high-power, and continuous-wave operation of distributed-feedback quantum-cascade lasers at 9.6 m
Appl. Phys. Lett. **88**, 201114 (2006); 10.1063/1.2205730

Surface-emitting 10.1 m quantum-cascade distributed feedback lasers
Appl. Phys. Lett. **75**, 3769 (1999); 10.1063/1.125450


This article is copyrighted as indicated in the article. Reuse of AIP content is subject to the terms at: http://scitation.aip.org/termsconditions. Downloaded to IP: 129.175.97.14 On: Mon, 22 Sep 2014 12:37:22

# High temperature, single mode, long infrared ($\lambda = 17.8\ \mu$m) InAs-based quantum cascade lasers

D. Chastanet,[1] A. Bousseksou,[1,a)] G. Lollia,[2] M. Bahriz,[2] F. H. Julien,[1] A. N. Baranov,[2] R. Teissier,[2,b)] and R. Colombelli[1,c)]
[1]*Institut d'Electronique Fondamentale, Univ. Paris Sud, UMR 8622 CNRS, 91405 Orsay, France*
[2]*Institut d'Electronique du Sud, Univ. Montpellier 2, UMR 5214 CNRS, 34095 Montpellier, France*

(Received 23 June 2014; accepted 21 August 2014; published online 19 September 2014)

We demonstrate quantum cascade lasers in the InAs/AlSb material system which operate up to 333 K (in pulsed regime) at $\lambda = 17.8\ \mu$m. They employ metal-metal optical waveguides and the threshold current density is 1.6 kA/cm$^2$ at 78 K. We also report distributed-feedback devices obtained using the same laser material *via* a 1$^{st}$-order Bragg grating inscribed in the sole top metallic contact. Spectral single mode operation with more than 20 dB side mode suppression ratio is achieved at a temperature of 300 K. Large wavelength tuning rates, of the order of 1.5 nm/K, are demonstrated. A wavelength coverage of 0.38 $\mu$m is achieved in single-mode regime over a temperature range of 255 K. © *2014 AIP Publishing LLC*. [http://dx.doi.org/10.1063/1.4895763]

The 4th atmospheric transparency window, located in the 16 $\mu$m–30 $\mu$m wavelength range, motivates the development of efficient laser devices in this spectral region. Quantum cascade (QC) lasers in the InAs/AlSb material system and operating at long-infrared (long-IR) wavelengths represent a very interesting solution due to the low electronic effective mass of InAs ($0.023 \cdot m_0$; $m_0$ is the electron mass), which provides elevated optical gains.[1,2] As shown in Ref. 3, the low electronic effective mass in the InAs wells leads to extremely low threshold current densities and almost room-temperature (RT) operation at $\lambda > 19\ \mu$m. We have also shown that in this wavelength range metal-metal (MM) waveguides,[4] which are typically employed for THz lasers,[8] are very efficient and yield reasonable far-fields (FFs), contrary to what is experienced at THz frequencies.[5] Since applications such as trace gas-sensing, high resolution spectroscopy, or heterodyne detection require single mode longitudinal operation, the next relevant development is the implementation of efficient distributed feedback (DFB) lasers.

On one hand, the use of metallic top gratings for surface-plasmon mid-IR DFB QC lasers has been demonstrated in Refs. 6 and 7. On the other hand, 1D and 2D photonic crystal THz QC lasers are based on the sole patterning of the top metallization.[8–11] In this letter, we build on this know-how to realize long-IR DFB InAs/AlSb QC lasers operating at $\lambda = 17$–$18\ \mu$m.

The semiconductor sample was grown on an n-InAs substrate, in a Riber Compact 21 solid source molecular beam epitaxy (MBE) reactor. A double etch-stop layer section composed of AlAsSb/InAs/AlSb (200/100/5 nm) was grown before the active region (AR) to enable a selective substrate removal for the implementation of a MM waveguide geometry. At these long-IR wavelengths, MM waveguides are a good alternative to standard dielectric ones employed at shorter mid-IR wavelengths. They also have the advantage of practicality since they avoid the growth of very thick semiconductor cladding layers whose thickness scales with the wavelength.

The laser contains 72 repetitions of the AR for a total thickness of 7 $\mu$m. The detailed layer sequence is (beginning with the injection barrier, layer thickness in Angstroms): **18**/139/**1.5**/111/**1.5**/102/**3**/99/**6**/91/**6**/85/**6**/84/**9**/84/**12**/90/**15**/91. Bold numbers refer to AlSb barriers, and the underlined layers are n-doped with silicon to $3 \times 10^{17}$ cm$^{-3}$. The AR is based on the design reported in Ref. 3—a 4-quantum-well active region with a direct radiative transition—with the following changes: an 8% increase of the InAs wells width, a 10% higher doping level, and a reduction of 3 Å of the AlSb injector barrier thickness. The latter modification has been introduced in order to increase the maximum current density, since the limited dynamical range was a limiting factor for the maximum operating temperature ($T_{max}$) in our previous structure design.[3] As described in Ref. 12, the maximum current flow through the injection barrier can be partially controlled by the minimum energy splitting ($\Omega$) between the ground state of the injector and the upper level of the radiative transition. Reducing the thickness barrier leads to higher $\Omega$. As a consequence, a higher maximum current density can be achieved.

The calculated losses of the Fabry-Pérot (FP) waveguide are $\alpha \sim 20\ \text{cm}^{-1}$. We have also estimated the facet reflectivity at 30%. This value is not far from what expected in a standard dielectric waveguide, since the optical thickness of the active region (7 $\mu$m physical thickness) is larger than the wavelength. These values for facet reflectivity and waveguide losses are similar to our previous results in Ref. 3. FP laser ridge resonators have been fabricated in a metal-metal waveguide geometry using the same protocol as in Ref. 3. The optoelectronic characterisation of a typical FP laser in pulsed mode is reported in Fig. 1. The laser operates up to a $T_{max}$ of 333 K, which is the highest reported value for QC lasers in this wavelength range. The increase of the maximum operating temperature is mainly due to the higher maximum current density in our laser device. The emission wavelength is

a)E-mail: adel.bousseksou@u-psud.fr
b)E-mail: roland.teissier@ies.univ-montp2.fr
c)E-mail: raffaele.colombelli@u-psud.fr

 © 2014 AIP Publishing LLC

This article is copyrighted as indicated in the article. Reuse of AIP content is subject to the terms at: http://scitation.aip.org/termsconditions. Downloaded to IP: 129.175.97.14 On: Mon, 22 Sep 2014 12:37:22

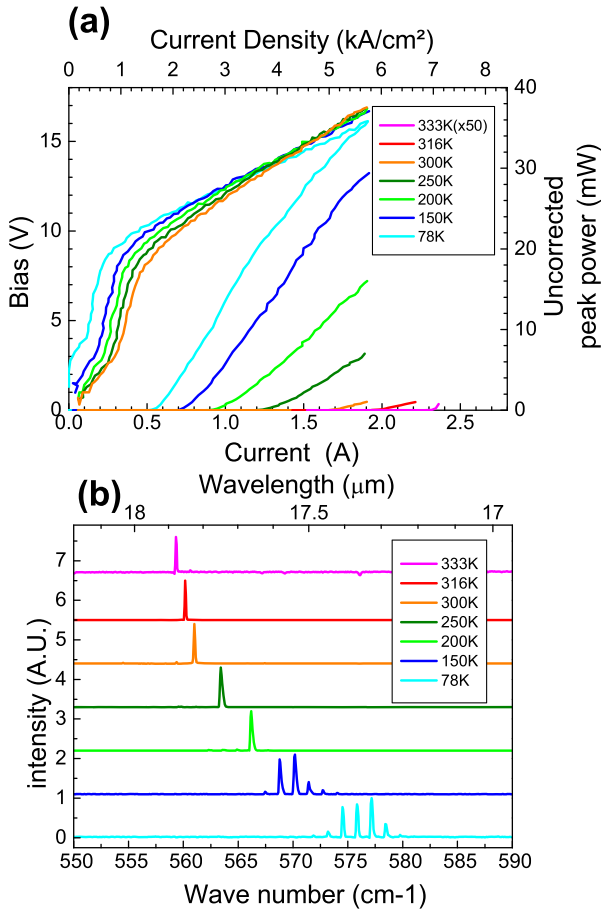


FIG. 1. Experimental results obtained on a FP sample under pulsed current injection (50 ns pulse width and 84 kHz repetition rate) using a FTIR equipped with an external Mercury Cadmium Telluride detector. The laser ridge dimensions are 1.5 mm × 22.8 $\mu$m. The output power was calibrated using a high sensitivity thermopile (*OPHIR 3A-SH*). The laser output was coupled to the power-meter through a ZnSe cryostat window (4 mm thick) and with two lenses (ZnSe 2 in. diameter, 1.5 in. focal and KBr 2 in. diameter and 2 in. focal). The uncorrected output peak power is the peak power collected from a single laser facet as it comes at the surface of the detector, no power correction is applied to overcome the optical absorption of optical windows and lenses used in our setup. We estimate that the transmission of our the optical setup is about 30% at 17–18 $\mu$m wavelength. (a) Current-Voltage and current-optical peak power characteristics at different heat-sink temperatures. (b) Emission spectra acquired at different heat-sink temperatures above laser threshold. The spectral resolution is 0.125 $cm^{-1}$.

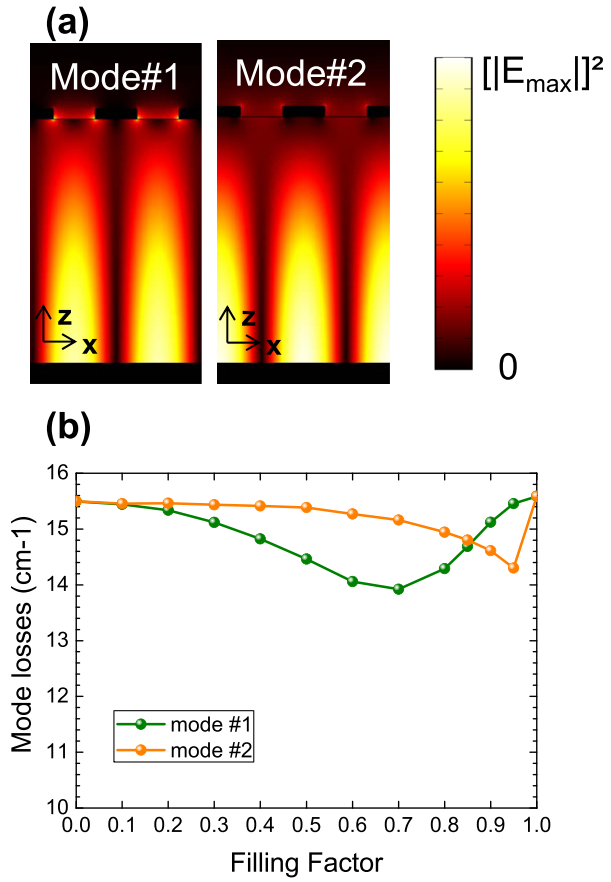


FIG. 2. 2D modeling of DFB devices (in-plane propagation direction). The calculations have been performed with a finite element based software in a single unit cell (i.e., one period of the grating), with Bloch periodic boundary conditions applied on the sides. (a) The figure shows the electromagnetic field intensity distribution of the symmetric and anti-symmetric modes along the x-z surface, for a grating with $ff = 0.5$. (b) Calculated optical mode losses of modes #1 and #2 as a function of the grating filling factor *ff*. The grating period is $\Lambda = 2.4$ $\mu$m. $ff = 0$ corresponds to no metallization of the device top surface. $ff = 1$ corresponds to full, unpatterned metallization.

centered at $\lambda = 17.37$ $\mu$m at 78 K, and it red-shifts to $\lambda = 17.75$ $\mu$m at RT (see typical spectra in Fig. 1(b)). The threshold current density ($J_{th}$) at 78 K is 1.6 kA/cm$^2$. This value is higher than in the previous active region design ($J_{th} = 0.6$ kA/cm$^2$). It mainly stems from an increased non-radiative leakage current channel, as described in Ref. 12.

Metal-metal waveguides ideally suit the implementation of 1D and 2D photonic crystals *via* the sole patterning of the top metallization.[6,10] Here, our goal is the implementation of a 1$^{st}$-order DFB grating. We have numerically simulated the field distribution (Fig. 2(a)) and the losses (Fig. 2(b)) as a function of the metal filling factor (*ff*) of the band-edge states at the 1st-order gap, where a 1st-order DFB laser operates. Contrary to what was observed for surface-plasmon mid-IR QC lasers,[13,14] where the grating induces the appearance of a low-loss mode, the field distributions and optical losses of the two modes are here very similar. This stems from the presence of the bottom metallic ground plane. The calculated losses, reported in Fig. 2(b), are very similar for the two modes, regardless of the grating filling-factor *ff*. Figure 2(b) shows that there is a weak optimum point for a grating with $ff = 0.7$. However, practical and technological reasons led us to choose $ff = 0.5$ in the present study.

The DFB device fabrication starts with Au-Au thermo-compressive wafer-bonding onto an InAs carrier wafer, followed by substrate and stop-layers removal with citric acid and an $HCl/H_2O_2/H_2O$ solution, respectively. The DFB metal grating was implemented via electron-beam lithography followed by Ti/Au (3/80 nm) metal coating and lift off.

25–35 $\mu$m-wide laser ridges were defined by contact optical lithography followed by wet chemical etching. An insulating layer (300 nm of $Si_3N_4$) was deposited by plasma enhanced chemical vapor deposition, and then opened on top of the ridges with reactive-ion etching. The deposition of the side top contact (Ti/Au), followed by sample thinning and back-contact metallization concludes the processing. Figure 3 shows a colorized scanning electron microscopy observation of a typical DFB device facet with $ff = 0.5$.

Figure 4 shows spectra, current-voltage (I-V), and current-output power (I-L) characteristics—in pulsed regime—from a

This article is copyrighted as indicated in the article. Reuse of AIP content is subject to the terms at: http://scitation.aip.org/termsconditions. Downloaded to IP: 129.175.97.14 On: Mon, 22 Sep 2014 12:37:22

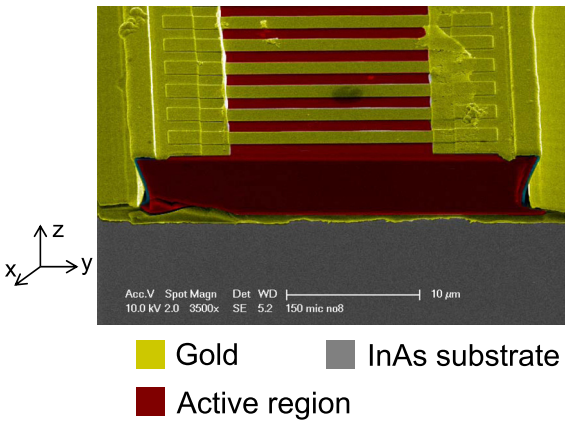


FIG. 3. The image shows a colorized scanning electron microscope image of the cleaved facet of a typical DFB laser. The red section corresponds to the active region (7 $\mu$m thick), the yellow ones to the Ti/Au metallic layers, and the blue section highlights the silicon nitride insulating layer.

typical DFB laser. The grating period is $\Lambda = 2.634\,\mu$m. The laser operates up to $T_{max} = 333$ K and the laser threshold at 78 K is $\approx 2$ kA/cm$^2$. The threshold increases with respect to the FP devices cannot be attributed to higher waveguide losses, since there is no significant difference in waveguide losses between DFB and FP cavities. The comparison of the calculated waveguide losses (2D calculation) is reported in Fig. 2(b) and it shows a maximum difference of 2 cm$^{-1}$ between a fully metallic waveguide and the lowest losses of a DFB resonator. We attribute, therefore, the observed threshold increase to (i) fabrication issues and (ii) mostly to a nonideal superposition between the active region peak gain and the Bragg grating mode of the DFB device. In fact, a comparison between the (central) emission wavelength of the FP and of the DFB devices (Figs. 1(b) and 4(b)) at a given temperature reveals a wavelength of about $\sim 0.15\,\mu$m at 333 K. Nevertheless, the $T_{max}$ is not drastically affected by the threshold increase.

As shown in Fig. 4(b), the laser spectra exhibit monomode operation with a Side Mode Suppression Ratio (SMSR) higher than 30 dB at 78 K (Fig. 4(c)). We also measured a SMSR higher than 20 dB at 300 K (data not shown). It is important to highlight that a single laser device shows continuous wavelength single mode tuning of 0.38 $\mu$m across a temperature span of 255 K (shown in Fig. 4(b)). The measured tuning rate as a function of the temperature is 1.5 nm/K, which leads to a refractive index variation of $2.85 \times 10^4$/K. This value is in very good agreement with values given for

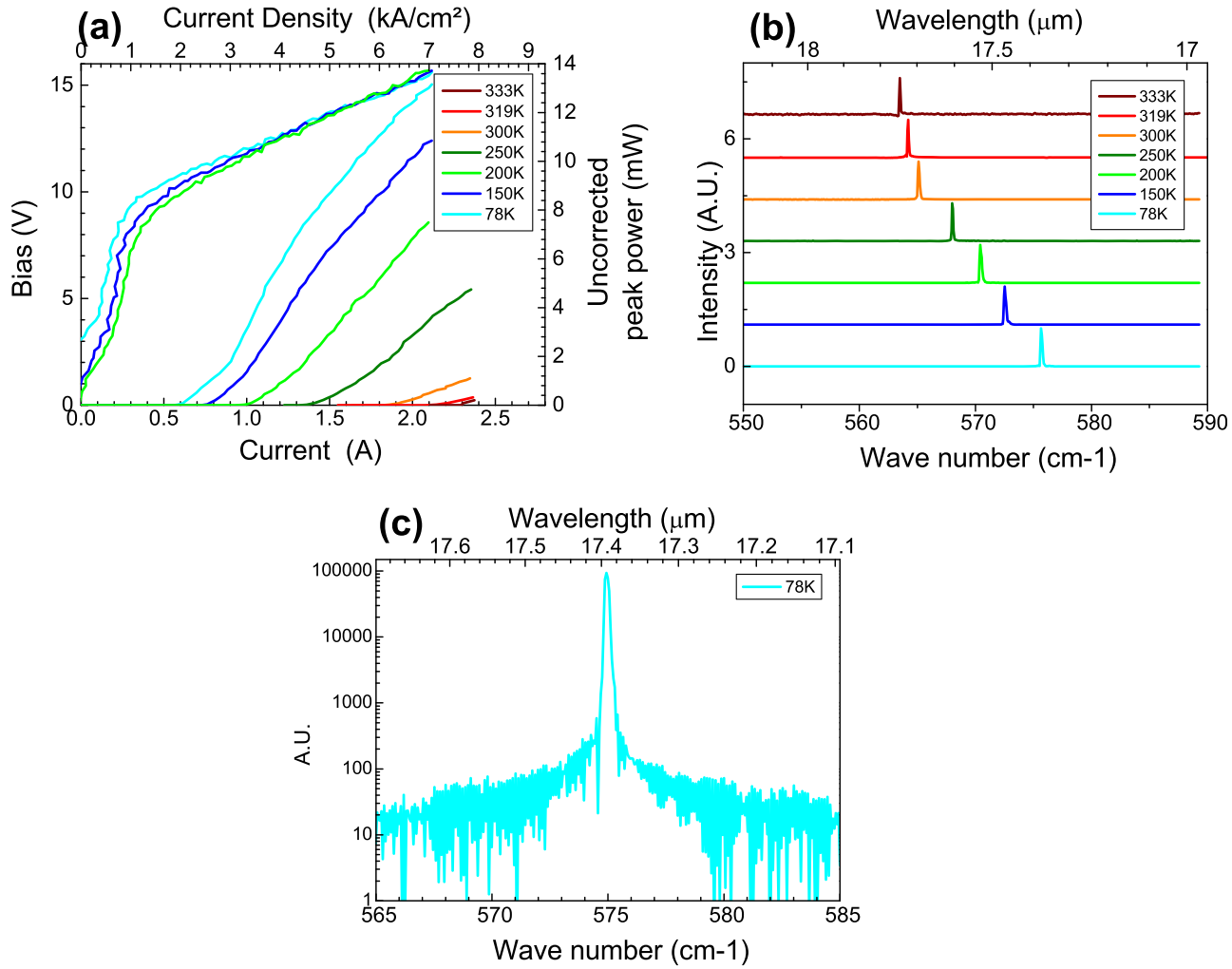


FIG. 4. Experimental results obtained on a DFB laser under pulsed current injection (50 ns pulse duration and 84 kHz repetition rate) using a Fourier transform IR spectrometer equipped with an MCT detector. The laser ridge dimensions are 1 mm $\times$ 30 $\mu$m. (a) I-V and I-L characteristics at different heat-sink temperatures. (b) Emission spectra acquired at different heat-sink temperatures above laser threshold. (c) Emitted spectrum in logarithmic scale at a temperature of 78 K. The spectral resolution is 0.125 cm$^{-1}$.

This article is copyrighted as indicated in the article. Reuse of AIP content is subject to the terms at: http://scitation.aip.org/termsconditions. Downloaded to IP: 129.175.97.14 On: Mon, 22 Sep 2014 12:37:22

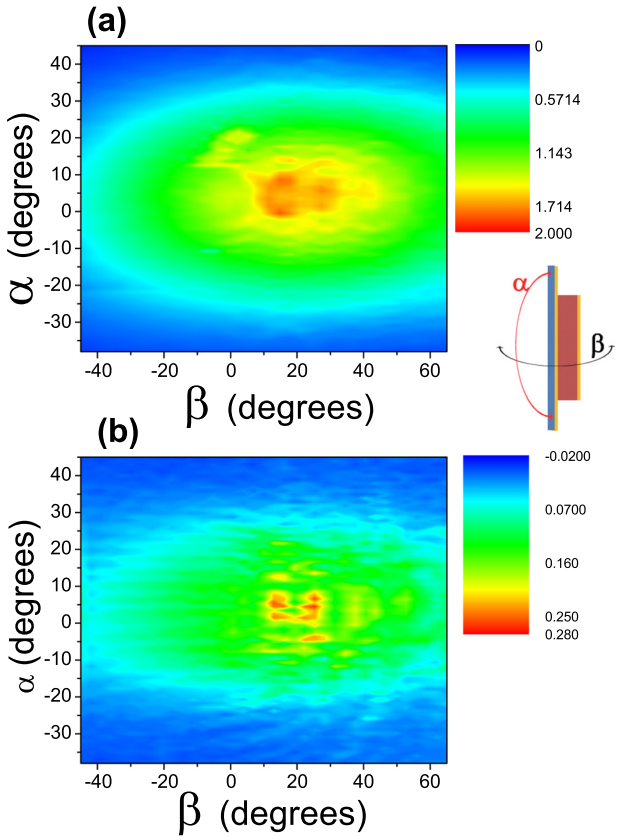


FIG. 5. Experimental far-field emission pattern of the FP (panel a) and of the DFB (panel b) lasers. The measurements are performed at 296 K using a liquid nitrogen cooled MCT detector. The setup maximum angular resolution is 0.57°. However, the far-fields have been acquired in steps of 3° along $\beta$ and 1° along $\alpha$.

InAs at $\lambda \sim 18\ \mu$m in Ref. 13. This tuning rate value is higher than for the InGaAs/AlInAs-on-InP material system (≈0.4 nm/K (Ref. 7)) and—crucially—it is close to the tuning rate of the peak gain as a function of temperature. This feature allows one to tune the DFB laser across a wide temperature range while ensuring single-mode operation. In other words, a single DFB device can cover a very wide wavelength range.

As a final characterization, we measured the FF emission patterns of the FP and DFB laser devices. The measurements were performed sweeping a liquid-nitrogen-cooled Mercury Cadmium Telluride detector on a 10-cm-radius sphere centered on the device facet. The angular resolution is ≈0.57°, but—to limit the acquisition time—the FFs have been acquired with 3° resolution along the vertical facet axis and with 1° resolution along the horizontal facet axis (see Fig. 5 for angular direction definitions). The measurements reveal that both devices operate on the fundamental $TM_{00}$ mode at room temperature. The FFs display a Gaussian-like pattern with similar divergences of 40° × 90°.

In conclusion, we have demonstrated high temperature operation of InAs based long-IR ($\lambda \sim 17.8\ \mu$m) QC lasers based on metal-metal optical waveguides. We have demonstrated single mode operation of 1st-order DFB devices obtained with the sole periodic patterning of the top metallization. The devices exhibit a side mode suppression ratio of 30 dB at 78 K (>20 dB at room temperature). A single DFB laser device achieves continuous wavelength tuning with temperature from $\lambda = 17.37$ to $\lambda = 17.75\ \mu$m. The tuning rate is 1.5 nm/K over the whole range 78 K – 333 K, and the device far-field is always well behaved. Such a wide tuning range could be particularly useful for spectroscopy applications.

We acknowledge financial support from the French National Research Agency (No. ANR-11-NANO-020 "DELTA") and from the Collaborative Action (No. 8748RA12) between the CEA and the University Paris Sud. This work was partly supported by the French RENATECH network. The device fabrication was performed at the nanocenter CTU-IEF-Minerve.

[1]O. Cathabard, R. Teissier, J. Devenson, J. Moreno, and A. N. Baranov, "Quantum cascade lasers emitting near 2.6 $\mu$m," Appl. Phys. Lett. **96**, 141110 (2010).
[2]M. Bahriz, G. Lollia, P. Laffaille, A. N. Baranov, and R. Teissier, "InAs/AlSb quantum cascade lasers operating near 20 $\mu$m," Electron. Lett. **49**, 1238 (2013).
[3]D. Chastanet, G. Lollia, A. Bousseksou, M. Bahriz, P. Laffaille, A. N. Baranov, F. H. Julien, R. Colembelli, and R. Teissier, "Long-infrared InAs-based quantum cascade lasers operating at 291K ($\lambda = 19\ \mu$m) with metal-metal resonators," Appl. Phys. Lett. **104**, 021106 (2014).
[4]K. Unterrainer, R. Colombelli, C. Gmachl, F. Capasso, H. Y. Hwang, A. M. Sergent, D. L. Sivco, and A. Y. Cho, "Quantum cascade lasers with double metal-semiconductor waveguide resonators," Appl. Phys. Lett. **80**, 3060–3062 (2002).
[5]E. Orlova, J. N. Hovenier, T. O. Klaassen, I. Kasalynas, A. J. L. Adam, J. R. Gao, T. M. Klapwijk, B. S. Williams, S. Kumar, Q. Hu, and J. L. Reno, Phys. Rev. Lett. **96**, 173904 (2006).
[6]A. Bousseksou, V. Moreau, R. Colombelli, C. Sirtori, G. Patriarche, O. Mauguin, L. Largeau, G. Beaudoin, and I. Sagnes, "Surface-plasmon distributed-feedback mid-infrared quantum cascade lasers based on hybrid plasmon/air-guided modes," Electron. Lett. **44**(13), 807–808 (2008).
[7]A. Bousseksou, R. Colombelli, A. Babuty, Y. De Wilde, Y. Chassagneux, C. Sirtori, G. Patriarche, G. Beaudoin, and I. Sagnes, "A semiconductor laser device for the generation of surface-plasmons upon electrical injection," Opt. Express **17**(11), 9391 (2009).
[8]C. Sirtori, S. Barbieri, and R. Colombelli, "Wave engineering with THz quantum cascade lasers," Nat. Photonics **7**, 691–701 (2013).
[9]J. A. Fan, M. A. Belkin, F. Capasso, S. Khanna, M. Lachab, A. G. Davies, and E. H. Linfield, "Surface emitting terahertz quantum cascade laser with a double-metal waveguide," Opt. Express **14**, 11672–11680 (2006).
[10]G. Xu, V. Moreau, Y. Chassagneux, A. Bousseksou, R. Colombelli, G. Patriarche, G. Beaudoin, and I. Sagnes, "Surface emitting quantum cascade lasers with metallic photonic-crystal resonators," Appl. Phys. Lett. **94**, 221101 (2009).
[11]G. Xu, R. Colombelli, S. P. Khanna, A. Belarouci, X. Letartre, L. Li, E. H. Linfield, A. G. Davies, H. Beere, and D. Ritchie, "Efficient power extraction in surface-emitting semiconductor lasers using graded photonic heterostructures," Nat. Commun. **3**, 952 (2012).
[12]C. Sirtori, F. Capasso, J. Faist, A. L. Hutchinson, D. L. Sivco, and A. Y. Cho, "Resonant tunneling in quantum cascade lasers," IEEE J. Quantum Electron. **34**(9), 1722–1729 (1998).
[13]A. Bousseksou, Y. Chassagneux, J. R. Coudevylle, R. Colombelli, C. Sirtori, G. Patriarche, G. Beaudoin, and I. Sagnes, "Surface-plasmon distributed-feedback quantum cascade lasers operating pulsed, room temperature," Appl. Phys. Lett. **95**, 091105 (2009).
[14]M. Bertolotti, V. Bogdanov, A. Ferrari, A. Jascow, N. Nazorova, A. Pikhtin, and L. Schirone, "Temperature dependence of the refractive index in semiconductors," J. Opt. Soc. Am. B **7**(6), 918–922 (1990).

This article is copyrighted as indicated in the article. Reuse of AIP content is subject to the terms at: http://scitation.aip.org/termsconditions. Downloaded to IP: 129.175.97.14 On: Mon, 22 Sep 2014 12:37:22